Phase behavior of charged colloids at a fluid interface

Colm P. Kelleher,[*] Rodrigo E. Guerra, Andrew D. Hollingsworth, and Paul M. Chaikin

Department of Physics and Center for Soft Matter Research, New York University, 4 Washington Place, New York,
New York 10003, USA

We study the phase behavior of a system of charged colloidal particles that are electrostatically bound to an almost flat interface between two fluids. We show that, despite the fact that our experimental system consists of only 10^3–10^4 particles, the phase behavior is consistent with the theory of melting due to Kosterlitz, Thouless, Halperin, Nelson, and Young. Using spatial and temporal correlations of the bond-orientational order parameter, we classify our samples into solid, isotropic fluid, and hexatic phases. We demonstrate that the topological defect structure we observe in each phase corresponds to the predictions of Kosterlitz-Thouless-Halperin-Nelson-Young theory. By measuring the dynamic Lindemann parameter $\gamma_L(\tau)$ and the non-Gaussian parameter $\alpha_2(\tau)$ of the displacements of the particles relative to their neighbors, we show that each of the phases displays distinctive dynamical behavior.

I. INTRODUCTION

Colloidal systems have long been used as a model for investigating fundamental questions in condensed matter physics. Two-dimensional (2D) systems are of particular interest, both for the rich physical phenomena they display [1,2] and for the ease with which they can be imaged, via video or confocal microscopy [3]. To create such a system, colloidal particles must somehow be confined to a surface. This can be done by using colloids sedimented onto a solid or fluid substrate [2,4,5], by physically confining colloids between the parallel walls of a thin sample chamber [1,6], or by using charged particles that bind electrostatically to a fluid interface [7,8]. The latter system has the advantage that the surface to which the particles bind does not have to be flat and so is particularly useful in exploring the role of background curvature in determining the structure and dynamics of topological defects in 2D materials [9,10]. However, the phase behavior of colloids in this kind of system, which is necessary for a full understanding of experiments undertaken at finite temperature, has not been investigated.

In this work, we study systems of 10^3–10^4 charged colloidal particles that are electrostatically bound to an almost-flat fluid interface, shown schematically in Fig. 1. We demonstrate that the interaction between particles is consistent with a dipolar pair potential. We measure the dipole moment of the particles, which allows us to directly compare the phase behavior of our system to previous experiments and simulations using dipolar particles [2,11,12].

Using density as the control parameter, we show that the phase behavior of our system is consistent with the theory of defect-mediated melting due to Kosterlitz, Thouless, Halperin, Nelson and Young, whereby the transition from isotropic fluid to crystalline solid happens via an intermediate hexatic phase [13–15]. We identify the solid, isotropic fluid, and hexatic phases by measuring the bond-orientational order parameter ψ_6 and associated space and time correlation functions $g_6(r)$ and $g_6(\tau)$. Finally, we show that the classification of our samples into solid, isotropic fluid, and hexatic phases is consistent both with the topological defect structure predicted by

Kosterlitz-Thouless-Halperin-Nelson-Young (KTHNY) theory and with the dynamical behavior that has been described previously [16].

II. MATERIALS AND METHODS

Our experimental system is composed of diameter $d = 1.1\ \mu$m poly(methyl methacrylate) (PMMA) particles that bind electrostatically to the interface between an oil and an aqueous phase. The particles are initially dispersed in a 1:1 volumetric mixture of cyclohexyl bromide (CHB) and dodecane, while the aqueous phase consists of a 10 mM solution of NaCl in a 90 wt. % glycerol-water mixture. The dielectric constant ϵ of the oil is $4.3\epsilon_0$, where ϵ_0 is the permittivity of the vacuum [17]. The CHB is purified and stored according to the protocols given in Refs. [7,18]. The PMMA particles are sterically stabilized with covalently bound poly(12-hydroxystearic acid) (PHS) [19]. Previous work has shown that, when dispersed in similar oils, micron-sized PHS-coated PMMA particles acquire a charge q of around $+500e$, where e is the elementary charge [7,20]. While the charging mechanism is still incompletely understood [18,21,22], particle charging in our system is robust and reproducible [20]. To facilitate measurement of particle dynamics with confocal microscopy, we fluorescently dye the particles with absorbed rhodamine 6G [23].

To prepare the particle-laden interfaces we use in our experiments, we use an atomizer to deposit droplets of the aqueous phase onto a cover slip. We then incorporate the cover slip into the construction of a glass capillary channel, which is filled with the particle dispersion at the desired concentration. As the particle dispersion flows into the chamber, some of the particles bind irreversibly to the surface of the droplets, while others bind to the bare glass surface. The experimental geometry is shown schematically in Fig. 1. Particles that are bound to the interface are mobile and can reach thermodynamic equilibrium. To control the flatness of the fluid interfaces, prior to the droplet deposition step, the cover slip is immersed in a bath of KOH-saturated isopropanol (IPA) and rinsed sequentially with deionized water, acetone, and IPA. The cover slip is blown dry with an N_2 sprayer and dried in an oven at $70\,^\circ$C for at least 15 min prior to use. By varying the immersion time of the cover slips in the KOH solution, we control the advancing contact

———————
[*]Corresponding author: cpk235@nyu.edu
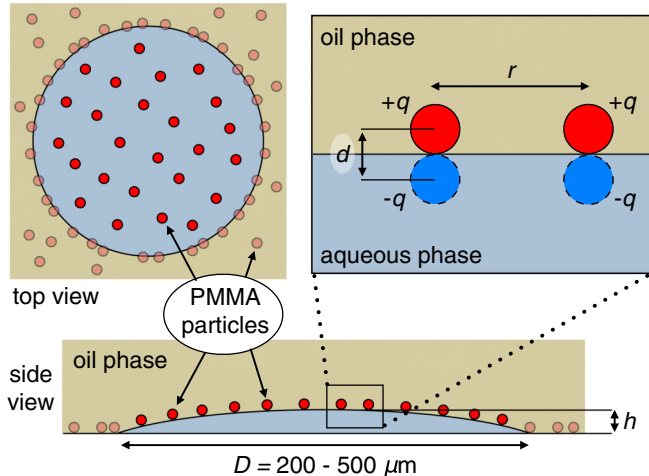
FIG. 1. Schematic of the experimental geometry. In the side view panel, the height h of the droplet is exaggerated compared to the base diameter D. In experimental samples, $h \lesssim 5 \ \mu$m. Particles sitting on the interface (shown in full color) are mobile, while the remaining particles (shown as faded) bind randomly and irreversibly to the bare glass surface. The boundary of the droplet is delineated by a row of particles stuck to the glass. The inset shows the origin of the dipolar repulsion between interfacial particles.

angle of the deposited droplets of the aqueous phase.[1] We find that immersing the cover slips for 30 min gives contact angles of approximately $1°$, which are appropriate for this experiment. Apart from the KOH immersion step, we follow the same protocol to clean all glass surfaces that come into contact with the particle dispersion. Once the capillary channel has been filled, we seal it: first with a buffer layer of glycerol and then with optical adhesive (Norland Products Inc. NOA 68).

Following the above procedures, we obtain a sample chamber that contains several particle-laden interfaces, ranging in base diameter D from around 200 to 500 μm. Each interface has a slightly different areal density ρ of PMMA particles, thus allowing us to approximately uniformly sample areal densities in the range 0.01–0.15 μm^{-2}. We estimate the curvature of the droplets as follows: Using a $10\times$ magnification, 0.3 numerical aperture air objective mounted on a Leica TCS SP5 II confocal microscope, we image the particles in a single confocal slice. If all the particles appear in the field of view, the maximum thickness of the drop must then be less than the optical section thickness, around 5 μm. Since the dimensions of our droplet are far smaller than the capillary length, we ignore the effect of gravity[2] and assume that the droplets take the shape of a spherical cap. Since $D > 200 \ \mu$m and the thickness is less than 5 μm, the radius of curvature must be at least 1 mm: far greater

---

[1]We speculate that the dramatic change in the wetting properties of glass cover slips upon immersion in KOH IPA is caused by gradual removal of residues left over from the manufacturing process, roughening of the glass surface upon contact with the base bath, or some combination of these mechanisms.

[2]Assuming the surface tension of our interface lies in the typical range for an interface between an oil phase and an aqueous phase, 20–50 mN m^{-1}, the capillary length is 0.3–0.5 cm.

than the length scales probed in our experiments. Thus, when analyzing our experimental data, we treat the droplet surface as flat.

After waiting at least a day for the samples to equilibrate, we use confocal microscopy to record the motion of the particles for up to several hours, at a rate of 0.25–1.0 frames/s. Using standard routines [24], we locate the particles in the field of view. Delaunay triangulations of the instantaneous particle positions identify sites with more or fewer than six nearest neighbors, called disclinations. Trajectories obtained by linking particle positions in adjacent frames reveal the mobility of individual particles.

Snapshots and movies of particle layers of different densities captured and analyzed in this way display the qualitative features of the three phases predicted by Kosterlitz, Thouless, Halperin, Nelson, and Young. The low-density isotropic fluid phase shown in Fig. 2(a) is characterized by homogeneously distributed disclination defects and uniformly mobile particles. By contrast, the high-density equilibrium crystal phase, shown in Fig. 2(c), is only capable of supporting sparse clusters of tightly bound defects that do not affect the long-range order of the lattice. In this phase, the particles that compose the crystal are uniformly confined to the vicinity of their lattice sites. As we show in Sec. III, the resulting caged diffusion can be used to measure *in situ* the strength of the interparticle interactions.

At intermediate particle densities, such as that shown in Fig. 2(b), isolated disclinations condense into the defect clusters that characterize the hexatic phase. These clusters facilitate particle mobility, disrupt translational order, and induce long-lived spatial inhomogeneities in the structure and dynamics of the particles.

III. MODEL FOR INTERPARTICLE INTERACTIONS AND MEASUREMENT OF DIPOLE MOMENT OF PARTICLES

To compare the phase behavior of our system with that observed in other systems [2,11,12,25], it is important to know both the form and magnitude of the interparticle repulsion [26]. In previous work, we studied the behavior of PHS-coated PMMA particles at an interface between two fluids that are similar in composition to those described here [20]. In our system, the PMMA particles appear to be wetted very little (or possibly not at all) by the aqueous phase and can be described as spheres with charge q sitting on top of a conducting medium, as shown in the inset in Fig. 1. In the same work, we showed that the force binding individual particles to the interface is electrostatic in origin and that the interaction between pairs of particles is dipolar. These results are consistent with previous experimental and theoretical work [27–29] on systems of charged particles in the vicinity of a fluid interface. In our system and similar ones, the interaction of two charged particles is the sum of the Coulomb repulsion between the particles and the Coulomb attraction between each particle and the image charge of the other. Thus, in the limit where the interparticle distance r is large compared to the diameter d of the particles, the net interaction between two interfacially bound particles can be approximated by a pair potential of the form

$$U(r) \simeq \frac{A}{r^3},$$
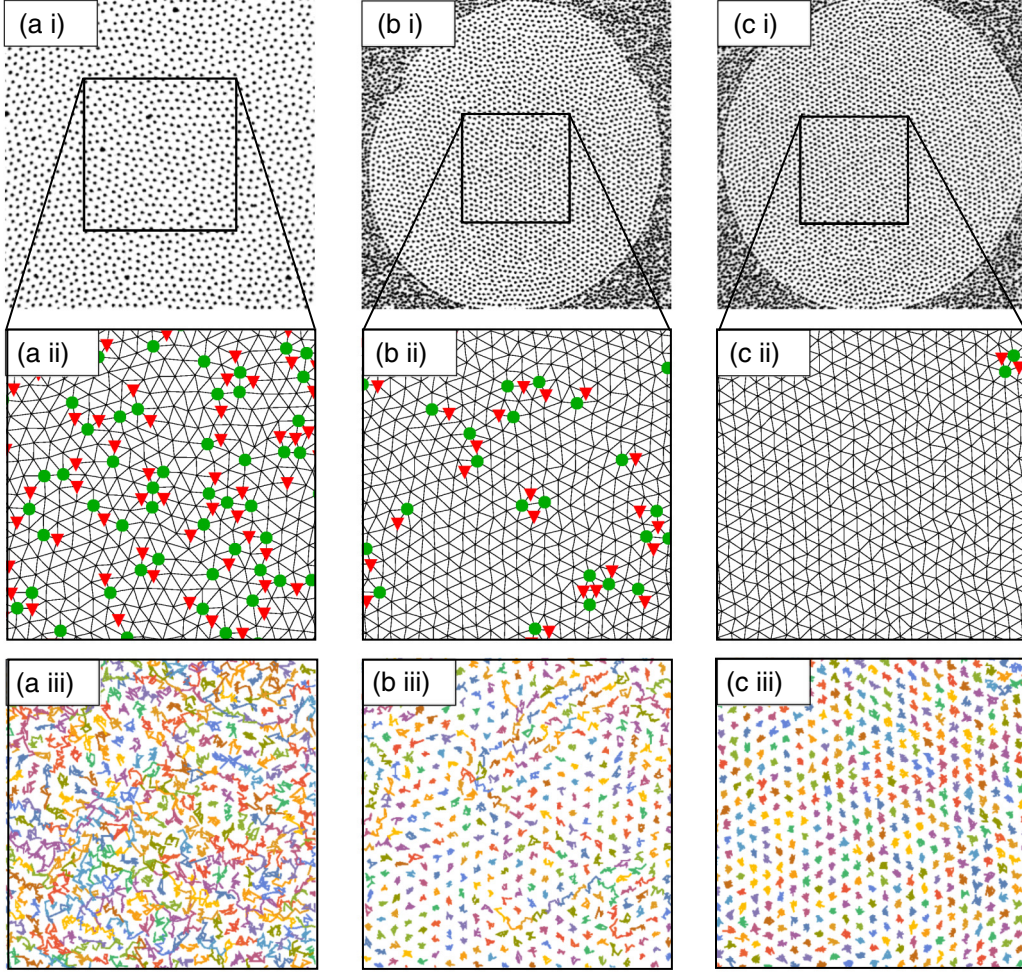
FIG. 2. Three samples of hydrophobic PMMA particles electrostatically bound to almost-flat droplets, at areal densities ρ of (a) 0.036, (b) 0.043, and (c) 0.049 μm^{-2}. The top row shows a confocal micrograph of each sample. For samples (b) and (c), the entire, roughly circular droplet is shown (see Fig. 1). In each sample, the inset square has a side length of 100 μm. The middle row shows Delaunay triangulations of the particle positions in a selected region, in the first frame of each movie. Particles with five or seven nearest neighbors are respectively indicated by red triangles and green disks. The bottom row shows the particle trajectories over 25 min.

where $A = p^2/8\pi\epsilon$, with $p = qd$ the magnitude of the electric dipole moment of the particles.[3] As shown in Fig. 2(c iii), when the interfacial density of the particles is high enough, they form a crystalline solid phase. In a hexagonal lattice composed of repulsive dipolar particles, the average value of p can be estimated by observing the fluctuations of the particles relative to the cage formed by their nearest neighbors. To quantify the interactions between our interfacial PMMA particles, we use a method due to Parolini *et al.* [30], which we now outline briefly.

We begin by identifying a region of the interface where several hundred particles are arranged in a defect-free crystal lattice that is at least 20 μm from the droplet boundary. We consider only samples where the density gradient across the subregion of interest is less than 0.3% per interparticle spacing and avoid the grain boundaries or isolated dislocations that are

occasionally present in our samples. These nonequilibrium features may be identified quantitatively, for instance, by anomalous behavior of the dynamic Lindemann parameter $\gamma_L(\tau)$ or the non-Gaussian parameter $\alpha_2(\tau)$, which we define in Sec. V. To further check that we are measuring equilibrium properties, we verify that our results do not depend strongly on the particular choice of subregion.

At each instant t in time, the Delaunay triangulation defines $\mathcal{N}_i$, the set of nearest neighbors of particle i. The position of particle i relative to its neighbors is given by

$$\mathbf{r}_{i,\text{NN}}(t) = \mathbf{r}_i(t) - \frac{1}{n_b} \sum_{j \in \mathcal{N}_i} \mathbf{r}_j(t),$$

where the sum is taken over the n_b neighbors of particle i. The nearest-neighbor relative mean square displacement (NNMSD) as a function of time interval τ is defined as

$$\langle \delta\mathbf{r}_{\text{NN}}(\tau)^2 \rangle = \langle [\mathbf{r}_{i,\text{NN}}(t+\tau) - \mathbf{r}_{i,\text{NN}}(t)]^2 \rangle, \qquad (1)$$

where the average is taken over particles i and starting times t. When calculating the quantity $\mathbf{r}_{i,\text{NN}}(t+\tau)$, we use the set of

---

[3]The latter relation assumes a constant charge density on the surface of the particle, but the dipolar form of the interaction holds even for more complicated boundary conditions on the surface of the particle.
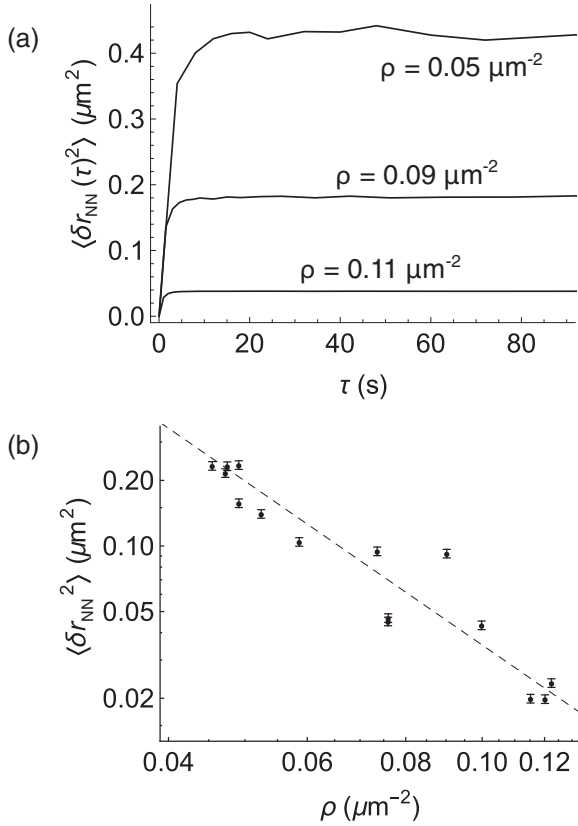
FIG. 3. (a) Nearest-neighbor relative mean square displacement curves for three crystalline samples, at different densities ρ. (b) A log-log plot of the limiting value of the NNMSD, as a function of areal density. The dashed line is the best-fit line with slope $-5/2$, as predicted by Eq. (2). This fit gives an electric dipole moment $p = (455 \pm 20)\, e\,\mu\text{m}$.

neighbors defined at time t, even if those particles no longer share a Delaunay bond with particle i at time $t + \tau$. Figure 3(a) shows $\langle \delta \mathbf{r}_{NN}(\tau)^2 \rangle$ curves for three crystalline samples, at different densities ρ. In all these samples, $\langle \delta \mathbf{r}_{NN}(\tau)^2 \rangle$ reaches a plateau value $\langle \delta \mathbf{r}_{NN}^2 \rangle$. According to [30], this value is related to the force constant A, and hence to the dipole moment p, by the equation

$$\langle \delta \mathbf{r}_{NN}^2 \rangle = \frac{2^{9/2} \alpha k_B T}{3^{5/4} A} \rho^{-5/2}, \qquad (2)$$

where we have used the relation between ρ and interparticle spacing a in a hexagonal lattice, $\rho = 2/a^2 \sqrt{3}$. The constant α is calculated in Ref. [30] and is approximately equal to 0.0531. Figure 3(b) shows the results of applying this method to ten crystalline samples at different areal densities. The error bars show the discrepancy between the results of calculating the limiting value of $\langle \delta \mathbf{r}_{NN}^2 \rangle$ in two different ways: first by using the plateau in the NNMSD curve as a function of time and second by computing the variance of the histogram of frame-to-frame displacements in the x and y directions separately. For a particle diffusing in an isotropic harmonic potential, sampled over sufficiently long times, these two methods should give the same result. Fitting the data to Eq. (2), we find that $p = (455 \pm 20)\, e\,\mu\text{m}$.

When discussing phase behavior in this system, it is convenient to introduce the dimensionless interaction parameter Γ,

$$\Gamma = \frac{A(\pi \rho)^{3/2}}{k_B T},$$

where $T = 293$ K is the temperature at which the experiments take place. Using Γ to describe the effective temperature of the system allows us to directly compare our results with previous experiments [2,31] and simulations [11] using dipolar repulsive particles.

IV. KTHNY THEORY: TOPOLOGICAL DEFECTS AND ORIENTATIONAL CORRELATIONS

Over the past several decades, KTHNY theory has been shown to describe the phase behavior of a broad class of 2D materials, including dipolar repulsive particles [26,32,33]. According to this theory, melting of a 2D crystalline solid takes place via two continuous transitions, which can be understood in terms of the topological defects present in the material. Two types of topological defects are important: disclinations, points that have a number of nearest neighbors other than six, and dislocations, bound pairs of one five-coordinated and one seven-coordinated disclination. A dislocation is characterized by a Burgers vector, which represents the magnitude and direction of the lattice distortion induced by the dislocation [34]. Some examples of these kinds of defects are shown in Figs. 4(a) and 4(b).

According to KTHNY theory, in the solid phase at equilibrium, no free topological defects are present. However, there may be thermally activated pairs of dislocations of opposite Burgers vector that are bound by an attractive potential. These kinds of structures, an example of which is shown in Fig. 4(c), are not topological, since they can occur via local rearrangements of the lattice. At sufficiently low Γ, this attraction can be overcome by thermal fluctuations and the dislocation pairs dissociate. Although the resulting free dislocations destroy the finite shear modulus of the crystal lattice, the resulting material is not an isotropic fluid, but rather a liquid crystalline hexatic phase. The transition to the isotropic fluid is completed when the dislocations themselves unbind into their constituent disclinations.
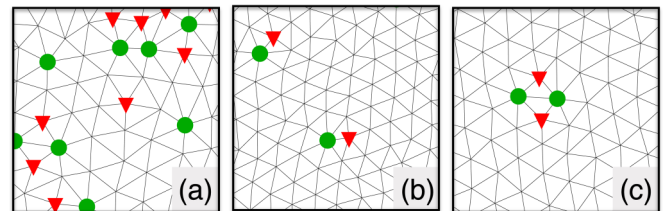
FIG. 4. Delaunay triangulations of typical particle configurations, taken from the samples shown in Fig. 2. Five- and seven-coordinated disclinations are marked by red triangles and green disks, respectively. Sample (a) shows three unpaired disclinations, while (b) shows two unpaired dislocations (five to seven pairs). Sample (c) shows a pair of dislocations with opposite Burgers vector. This configuration is not a topological defect.

TABLE I. Topological defect structure and properties of correlation functions $g_6(r)$ and $g_6(\tau)$ in the solid, hexatic, and fluid phases, according to KTHNY theory.

	Isotropic fluid	Hexatic	Solid
topological defects	free disclinations	free dislocations	none
$\lim\limits_{r \to \infty} g_6(r) \propto$	$\exp(-r/\xi_6)$	$r^{-\eta_6}$	const
$\lim\limits_{\tau \to \infty} g_6(\tau) \propto$	$\exp(-\tau/\tau_6)$	$\tau^{-\eta_6/2}$	const

Using data from experiments and simulations, different groups have explored various ways of quantitatively testing the predictions of KTHNY theory [25,35]. Of particular interest is the bond-orientational order parameter ψ_6, since it can be easily calculated from real-space data and because the functional form of the associated correlation functions $g_6(r)$ and $g_6(\tau)$ clearly discriminates between the phases of the material.

If particle k has position $\mathbf{r}_k$ at time t, the bond-orientational order parameter $\psi_6(\mathbf{r}_k,t)$ is then defined by

$$\psi_6(\mathbf{r}_k,t) = \frac{1}{n_b} \sum_{j \in \mathcal{N}_k} e^{6i\theta_{kj}},$$

where the sum is taken over the n_b nearest neighbors of particle k. The angle between particle k and its jth neighbor, θ_{kj}, is taken with respect to an arbitrary but fixed axis. The degree of local hexagonal order is given by $|\psi_6|$. In the crystal phase, the orientation of the hexagonal unit cell is given by $\frac{1}{6} \arg \psi_6$. The space and time correlation functions $g_6(r)$ and $g_6(\tau)$ are defined

$$g_6(r) = \mathrm{Re}\{\langle \psi_6^*(\mathbf{r}_k,t)\psi_6(\mathbf{r}_l,t)\rangle_{|\mathbf{r}_k - \mathbf{r}_l|=r}\},$$

$$g_6(\tau) = \mathrm{Re}\{\langle \psi_6^*(\mathbf{r}_k,t)\psi_6(\mathbf{r}_k,t+\tau)\rangle\}.$$

When calculating $g_6(r)$, the averages are taken over time and pairs of particles $\{k,l\}$ satisfying the condition $|\mathbf{r}_k - \mathbf{r}_l| = r$. For $g_6(\tau)$, the averages are taken over all particles k and starting times t. Thus, $g_6(r)$ is a two-particle correlation function, while $g_6(\tau)$ is a single-particle quantity. According to KTHNY

theory, these correlation functions have distinct behaviors in each of the three phases: For large r and τ, both functions tend to a constant value in the solid phase, decay algebraically in the hexatic phase, and decay exponentially in the isotropic fluid, with a characteristic decay length (time) ξ_6 (τ_6). Kosterlitz-Thouless-Halperin-Nelson-Young theory predicts that, in the hexatic phase, the exponent η_6 of the power-law decay of $g_6(r)$ is twice the exponent of the power-law decay of $g_6(\tau)$ and further dictates that, at the fluid-hexatic transition, η_6 reaches a critical value of $-1/4$ [32]. Some of these predictions are summarized in Table I.

Figures 5(a) and 5(b) respectively show $g_6(r)$ and $g_6(\tau)$, plotted for nine samples at values of Γ ranging from 53 to 91. In our analysis of the temporal correlation function $g_6(\tau)$, we rescale τ by the average time τ_0 required for a freely diffusing particle to traverse the mean distance between particles a. This step is necessary because the thickness of the aqueous layer underneath the particles (see Fig. 1) varies between samples. Thus, even in the limit of very low particle density, different samples may have diffusion coefficients D_0 that vary by as much as a factor of 4. We estimate τ_0 from the small-time behavior of the NNMSD curves, such as those shown in Fig. 3. At the smallest time intervals for which we have data, we assume that the particle is freely diffusing inside its cage of nearest neighbors and fit the first two data points of the $\langle \delta \mathbf{r}_{NN}(\tau)^2 \rangle$ curve by a straight line, containing the origin, with slope $4D_0$.[4] This allows us to estimate the time for a freely diffusing particle to traverse one interparticle spacing, $\tau_0 = a^2/4D_0$. For our samples, τ_0 is of order 30 min.

---

[4]The low temporal resolution of our data affects the accuracy of determining D_0 in this way. For particles in the solid phase, a more accurate determination of D_0 is available by fitting the mean square displacement curves to a more elaborate model [36]. Comparing the values of D_0 thus obtained to the values obtained by our short-time linear-fit method, we estimate that the error incurred by our method is at most around 50% and typically significantly smaller. This error, although systematic, is far smaller than the variation in the (unrescaled) particle mobilities.
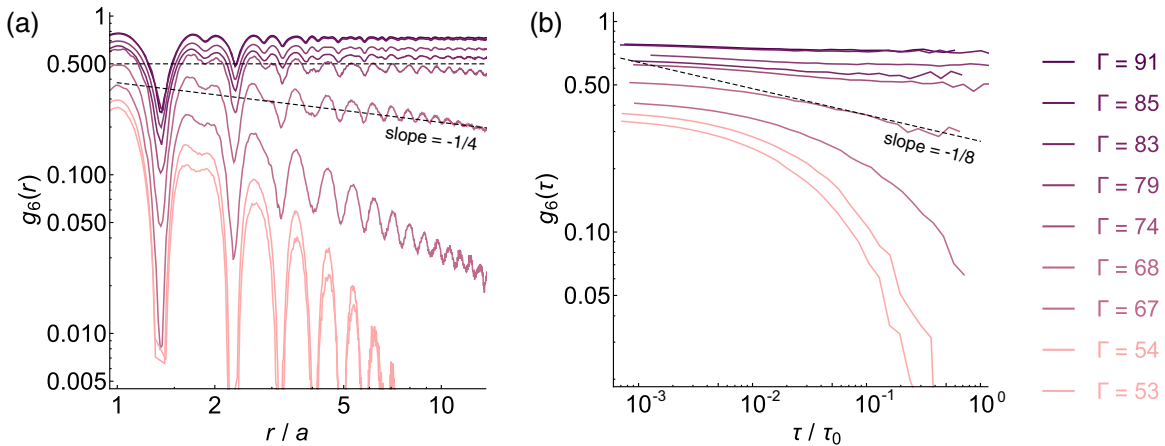
FIG. 5. Shown are log-log plots of orientational correlation functions $g_6(r)$ and $g_6(\tau)$, for nine samples at different values of Γ. The sloped dashed lines in each plot indicate algebraic decay with the exponents expected at the fluid-hexatic transition, while the horizontal dashed line in the $g_6(r)$ plot separates the curves that decay ($\Gamma \leqslant 74$) from those that reach a constant value ($\Gamma \geqslant 79$). Using these curves, we identify the fluid-hexatic and solid-hexatic transitions at $\Gamma_{FH} = 68 \pm 2$ and $\Gamma_{HS} = 76 \pm 3$.

For samples with $\Gamma \lesssim 67$, both $g_6(r)$ and $g_6(\tau)$ show the exponential decay characteristic of the isotropic fluid phase, while for $\Gamma \gtrsim 79$, both functions tend to a constant value at large r and τ. For the sample at $\Gamma = 74$, $g_6(r)$ shows behavior consistent with the power-law decay expected in the hexatic phase. For $\Gamma = 68$, the slope of $g_6(r)$ equals the critical value of $-1/4$ within experimental error and so we cannot unambiguously assign this sample to either phase. As can be seen from Fig. 5(b), for the samples at $\Gamma = 68$ and $\Gamma = 74$, our data for $g_6(\tau)$ do not allow us to distinguish between algebraic decay with a small negative power and a constant value. Thus, we estimate that the transition between the hexatic and the isotropic fluid phases occurs at $\Gamma_{\mathrm{FH}} = 68$ and the transition between the hexatic and the ordered phase occurs at $\Gamma_{\mathrm{HS}} = 76$.

We also note that the $g_6(r)$ and $g_6(\tau)$ curves for the $\Gamma = 79$ sample lie above those for the sample at $\Gamma = 83$, indicating that the former sample is more ordered. This apparent nonmonotonic behavior might reflect sample-to-sample variation in electric dipole moment p, which would cause experimental uncertainty in our calculated values of Γ and may also account for some of the spread of the data in Fig. 3. In fact, since the limiting values of the correlation functions should be a monotonic function of Γ, we can use the deviation from monotonicity to estimate the uncertainty in our stated values of Γ. Doing this, we find that the uncertainty in Γ is approximately 3%. This figure only accounts for sample-to-sample variation: The uncertainty in the mean value of the electric dipole moment p calculated from the data in Fig. 3 could lead to all the stated values of Γ being shifted systematically from their true values by as much as 8%. In spite of these experimental uncertainties, the values of Γ_{FH} and Γ_{HS} that we find are in quantitative agreement with those found in previous experiments [12,16].

The final orientational quantity we define is the average orientational order parameter $\Psi_6 = \langle \psi_6(\mathbf{r}_k, t) \rangle$, where the average is taken over all points k and times t. We expect that, in the isotropic fluid phase, $|\Psi_6| = 0$, while in the crystalline solid phase, $|\Psi_6|$ takes a finite positive value, which tends to unity as Γ increases. In Fig. 6(a) we plot $|\Psi_6|$ as a function of interaction parameter Γ. Figure 6(b) shows the total defect fraction, defined as the fraction of particles that have a number of nearest neighbors other than six. Between Γ_{FH} and Γ_{HS}, the defect fraction drops dramatically and we see a corresponding growth in the orientational order $|\psi_6|$ in the system.

Figure 6(c) shows a plot of the fraction of unpaired dislocations n_{disloc} and disclinations n_{disc}. A topological defect is defined as unpaired if it is does not share a Delaunay bond with any other defect. Thus, the five-coordinated disclination in the center of Fig. 4(a) is unpaired, as are the two dislocation defects in Fig. 4(b). On the other hand, both the cluster of defects in the top right of Fig. 4(a) and the two adjacent dislocations of opposite Burgers vector in Fig. 4(c) are paired and neither contributes to n_{disloc} or n_{disc}. While computationally straightforward, our definition of *unpaired* defects does not provide a direct measurement of the concentration of *free* defects in the sense of KTHNY theory. This is true for at least two reasons. First, our definitions of n_{disloc} and n_{disc} treat energetically bound but nonadjacent defects as unpaired. This leads us to overestimate the number of free defects, especially in the solid and hexatic phases. Second,
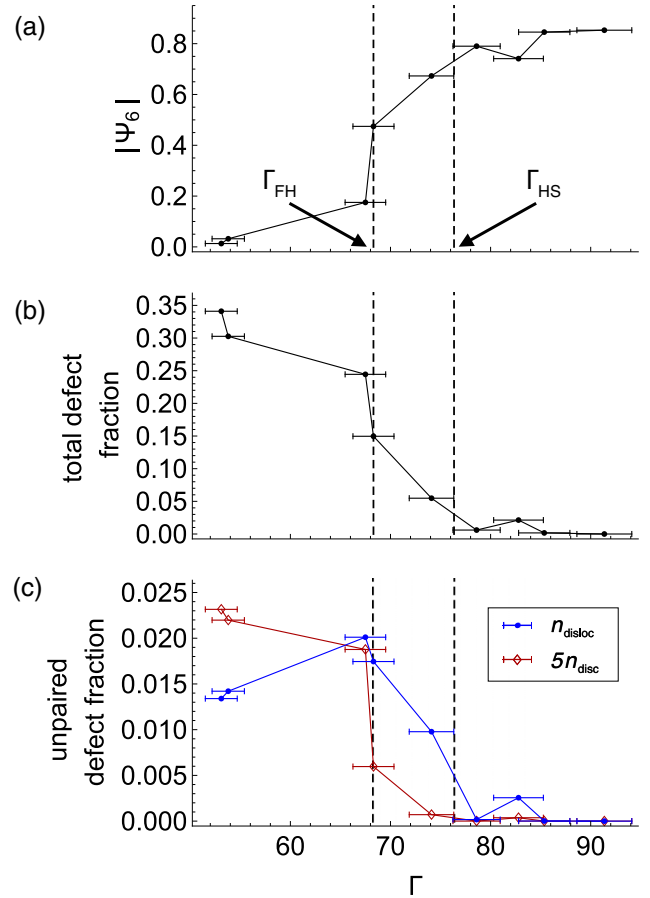
FIG. 6. (a) Absolute value of the average bond-orientational order parameter, plotted as a function of the interaction parameter Γ. The dashed lines indicate the values of Γ at the fluid-hexatic and hexatic-solid transitions, as defined by the behavior of the correlation functions $g_6(r)$ and $g_6(\tau)$ (see Fig. 5). (b) Fraction of particles that do not have six nearest neighbors. (c) Fraction of particles that form unpaired disclinations or dislocations. To enable these quantities to be displayed on the same plot, the fraction of unpaired disclinations is multiplied by a factor of 5.

our definitions completely neglect defect clusters, such as the structure in the top right of Fig. 4(a), which may contain one or several net topological defects. This will cause us to underestimate the number of free defects, especially in the fluid phase, where such clusters proliferate. Despite these shortcomings, we find that n_{disloc} and n_{disc} display the expected behavior in the vicinity of the transitions: Near $\Gamma = \Gamma_{\mathrm{FH}}$, n_{disc} drops dramatically, while near $\Gamma = \Gamma_{\mathrm{HS}}$, n_{disloc} does the same.

V. DYNAMICAL MEASURES OF PHASE BEHAVIOR

As well as displaying distinctive spatial structure, different phases of a material are typically characterized by their dynamics. To investigate this aspect of the phase behavior of our samples, we plot, in Fig. 7, the dynamic Lindemann parameter $\gamma_L(\tau)$ and the non-Gaussian parameter $\alpha_2(\tau)$ [16]. The dynamic Lindemann parameter $\gamma_L(\tau)$ is defined

$$\gamma_L(\tau) = \frac{\langle \delta \mathbf{r}_{\mathrm{NN}}(\tau)^2 \rangle}{2a^2}, \qquad (3)$$
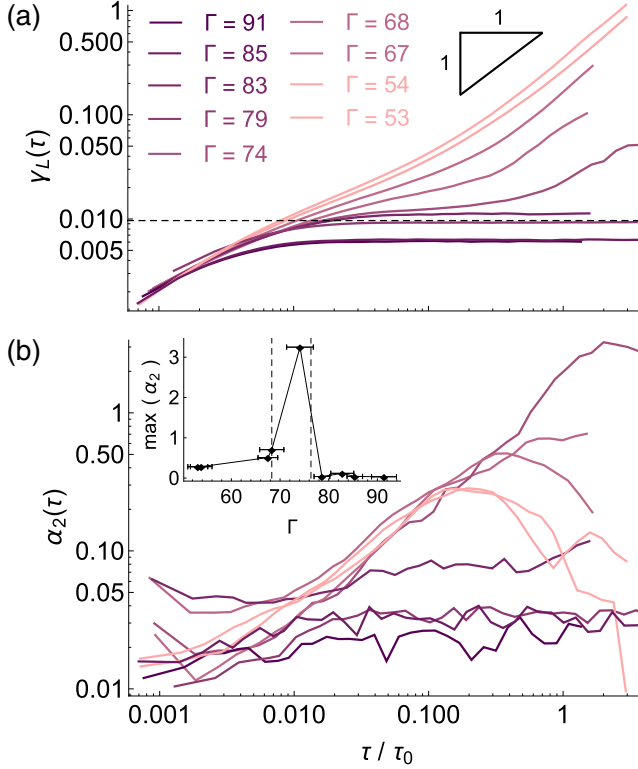
FIG. 7. Shown are log-log plots of (a) the dynamic Lindemann parameter $\gamma_L(\tau)$ and (b) the non-Gaussian parameter $\alpha_2(\tau)$. Panel (a) shows that, for samples identified as belonging to the ordered phase by our analysis of the correlation functions, $\gamma_L(\tau)$ reaches a constant value, while the samples with $\Gamma < \Gamma_{HS}$ behave diffusively or subdiffusively. The horizontal dashed line indicates the critical value $\gamma_L^c = 0.0097$ predicted by Eqs. (2) and (3), evaluated at the density ρ_{HS} corresponding to Γ_{HS}. Panel (b) shows that, in the isotropic fluid, α_2 peaks at some intermediate time scale, while in the candidate hexatic samples ($\Gamma = 68$ and 74), non-Gaussian behavior grows over the time scales we observe. The inset in (c) highlights the dramatic growth in the maximum value of α_2 in the hexatic phase. The vertical dashed lines indicate Γ_{FH} and Γ_{HS}, as defined by the behavior of the correlation functions $g_6(r)$ and $g_6(\tau)$.

where the NNMSD $\langle \delta \mathbf{r}_{NN}(\tau)^2 \rangle$ is defined in Eq. (1). The non-Gaussian parameter $\alpha_2(\tau)$ is defined as

$$\alpha_2(\tau) = \frac{\langle \delta \mathbf{r}_{NN}(\tau)^4 \rangle}{2 \langle \delta \mathbf{r}_{NN}(\tau)^2 \rangle^2} - 1.$$

This quantity measures the extent to which the histogram of particle displacements deviates from the normal distribution. Using the phase classification based on the behavior of the correlation functions $g_6(r)$ and $g_6(\tau)$, our measurements of $\gamma_L(\tau)$ and $\alpha_2(\tau)$ are consistent with previous measurements of the dynamics of systems in the solid, fluid, and hexatic phases [16].

In the solid phase, the dynamic Lindemann parameter reaches a plateau value at long time. The observed critical value of the dynamic Lindemann parameter is $\gamma_L^c = 0.012 \pm 0.001$. This is close to the value predicted by evaluating Eqs. (2) and (3) at the density ρ_{HS} corresponding to the hexatic-solid transition, $\gamma_L^c = 0.0097 \pm 0.005$. This comparison serves as a

consistency check on Eq. (2) and the measured value of Γ_{HS}. In the solid phase, the non-Gaussian parameter $\alpha_2(\tau)$ has a small positive value independent of time. This may be because the quantities $\mathbf{r}_{i,NN}$ are not statistically independent, as they take into account the positions of the nearest neighbors.

In the fluid phase, we observe diffusive behavior $\gamma_L(\tau) \propto \tau$ at long times, while the non-Gaussian parameter $\alpha_2(\tau)$ displays a local maximum at time intervals $\tau/\tau_0 \sim 0.1$. These time scales also correspond to the presence of a shoulder in the $\gamma_L(\tau)$ curves and are also similar to the characteristic times τ_6 of the exponential decay of the $g_6(\tau)$ curves shown in Fig. 5. All these time scales may originate in collective rearrangements of defect clusters, such as that shown in Fig. 4(a).

In the sample we identify as belonging unambiguously to the hexatic phase ($\Gamma = 74$), $\gamma_L(\tau)$ behaves subdiffusively over observed times. For the sample at $\Gamma = 68$, the correlation functions $g_6(r)$ and $g_6(\tau)$ are consistent with critical behavior and we are unable to assign it to either the fluid or the hexatic phase. For this sample, the slope of $\gamma_L(\tau)$ appears to be approaching 1 at the longest times we measure, perhaps indicating that it is indeed a fluid. Previously, Zahn and Maret showed that $\alpha_2(\tau)$ tends to a constant value of order unity for systems in the hexatic phase [16]. Our data are consistent with this finding, but we do not record our candidate hexatic samples for sufficiently long times to verify the limiting behavior. We do however observe the sharp growth in the maximum value of $\alpha_2(\tau)$ in the hexatic phase that was reported in the same study.
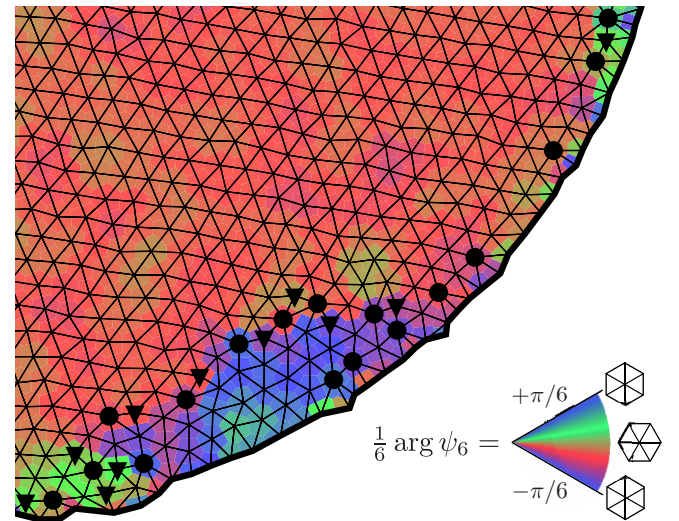
FIG. 8. Plot of the Delaunay triangulation of interfacially bound particles in a single quadrant of a roughly circular droplet. This sample has $\Gamma = 120$ and approximately 2000 particles in total. The color map shows the local orientation of the lattice, given by $\frac{1}{6} \arg \psi_6$, while five- and seven-coordinated disclinations are indicated by triangles and disks, respectively. The thick black curve identifies the droplet edge. (Disclinations are not plotted for the particles on the boundary.) Away from the edge, the system forms a monocrystal that spans the interior of the droplet. Immediately adjacent to the droplet edge, the lattice is aligned with the edge. Where the orientation of the interior region does not match that of the edge, grain boundaries form, a few lattice spacings from the boundary. These grain boundaries are delineated by a chain of polarized dislocations (five to seven pairs).

VI. CONCLUSION

In this work, we study a system of charged colloidal particles that are electrostatically bound to a fluid interface and interact via electric dipole-dipole repulsion. We show that the phase behavior of this system is well described by KTHNY theory, with density as the control parameter. Using the orientational correlation functions $g_6(r)$ and $g_6(\tau)$, we assign each sample to the solid, isotropic fluid, or hexatic phase. We demonstrate that the concentration of unpaired dislocations and disclinations is consistent with the KTHNY picture of defect-mediated melting. Finally, we find that each phase displays distinctive dynamical behavior, as measured by the dynamic Lindemann parameter $\gamma_L(\tau)$ and the non-Gaussian parameter $\alpha_2(\tau)$.

Given the small number of particles in our system, the extent to which our data are well modeled by KTHNY theory is quite surprising. This agreement is only possible because the orientation of the droplet edge, which is delineated by a line of pinned particles (see Fig. 2), does not propagate into the interior of the droplet. In the fluid phase, this is expected, since orientational correlations decay exponentially over lengths of a few interparticle spacings; this decay is evident in the $\Gamma \leqslant 67$ curves in Fig. 5(a). In the crystal phase, as shown in Fig. 8, the orientation inherited from the droplet edge is destroyed by a series of grain boundaries that run around the inner perimeter of the droplet. These grain boundaries separate an interior monocrystalline region from an outside layer, a few interparticle spacings wide, which is aligned with the edge of the droplet. Evidently, the strain fields associated with these grain boundaries are not large enough to significantly disrupt the phase behavior of the material in the interior region. In the hexatic, it is not immediately clear how the system accommodates the presence of the droplet edge, since grain boundaries are difficult to identify unambiguously in this phase.

The concurrence between our findings and previous work on larger systems of dipolar repulsive particles extends to quantitative agreement on the transition values of the interaction parameter Γ [2,12], although the sparsity our data, as well as the error bars for Γ shown, for example, in Fig. 6, limits our ability to determine the width of the hexatic window.

[1] C. A. Murray, W. O. Sprenger, and R. A. Wenk, Comparison of melting in three and two dimensions: Microscopy of colloidal spheres, Phys. Rev. B **42**, 688 (1990).

[2] K. Zahn, R. Lenke, and G. Maret, Two-Stage Melting of Paramagnetic Colloidal Crystals in Two Dimensions, Phys. Rev. Lett. **82**, 2721 (1999).

[3] J. C. Crocker and D. G. Grier, Methods of digital video microscopy for colloidal studies, J. Colloid Interface Sci. **179**, 298 (1996).

[4] R. Bubeck, C. Bechinger, S. Neser, and P. Leiderer, Melting and Reentrant Freezing of Two-Dimensional Colloidal Crystals in Confined Geometry, Phys. Rev. Lett. **82**, 3364 (1999).

[5] T. O. E. Skinner, D. G. A. L. Aarts, and R. P. A. Dullens, Grain-Boundary Fluctuations in Two-Dimensional Colloidal Crystals, Phys. Rev. Lett. **105**, 168301 (2010).

[6] Z. Zheng, F. Wang, and Y. Han, Glass Transitions in Quasi-Two-Dimensional Suspensions of Colloidal Ellipsoids, Phys. Rev. Lett. **107**, 065702 (2011).

[7] M. E. Leunissen, A. van Blaaderen, A. D. Hollingsworth, M. T. Sullivan, and P. M. Chaikin, Electrostatics at the oil-water interface, stability, and order in emulsions and colloids, Proc. Natl. Acad. Sci. USA **104**, 2585 (2007).

[8] W. T. M. Irvine, A. D. Hollingsworth, D. G. Grier, and P. M. Chaikin, Dislocation reactions, grain boundaries, and irreversibility in two-dimensional lattices using topological tweezers, Proc. Natl. Acad. Sci. USA **110**, 15544 (2013).

[9] W. T. M. Irvine, V. Vitelli, and P. M. Chaikin, Pleats in crystals on curved surfaces, Nature (London) **468**, 947 (2010).

[10] W. T. M. Irvine, M. J. Bowick, and P. M. Chaikin, Fractionalization of interstitials in curved colloidal crystals, Nat. Mater. **11**, 948 (2012).

[11] S. Z. Lin, B. Zheng, and S. Trimper, Computer simulations of two-dimensional melting with dipole-dipole interactions, Phys. Rev. E **73**, 066106 (2006).

[12] S. Deutschländer, A. M. Puertas, G. Maret, and P. Keim, Specific Heat in Two-Dimensional Melting, Phys. Rev. Lett. **113**, 127801 (2014).

[13] J. M. Kosterlitz and D. J. Thouless, Ordering, metastability and phase transitions in two-dimensional systems, J. Phys. C **6**, 1181 (1973).

[14] A. P. Young, Melting and the vector Coulomb gas in two dimensions, Phys. Rev. B **19**, 1855 (1979).

[15] B. I. Halperin and D. R. Nelson, Theory of Two-Dimensional Melting, Phys. Rev. Lett. **41**, 121 (1978).

[16] K. Zahn and G. Maret, Dynamic Criteria for Melting in Two Dimensions, Phys. Rev. Lett. **85**, 3656 (2000).

[17] H. Looyenga, Dielectric constants of heterogeneous mixtures, Physica **31**, 401 (1965).

[18] D. J. Evans, A. D. Hollingsworth, and D. G. Grier, Charge renormalization in nominally apolar colloidal dispersions, Phys. Rev. E **93**, 042612 (2016).

[19] M. T. Elsesser and A. D. Hollingsworth, Revisiting the synthesis of a well-known comb-graft copolymer stabilizer and its application to the dispersion polymerization of poly(methyl methacrylate) in organic media, Langmuir **26**, 17989 (2010).

[20] C. P. Kelleher, A. Wang, G. I. Guerrero-García, A. D. Hollingsworth, R. E. Guerra, B. J. Krishnatreya, D. G. Grier, V. N. Manoharan, and P. M. Chaikin, Charged hydrophobic colloids at an oil-aqueous phase interface, Phys. Rev. E **92**, 062306 (2015).

[21] M. E. Leunissen, Manipulating colloids with charges and electric fields. PhD. thesis, Utrecht University, 2007.

[22] M. N. van der Linden, J. C. P. Stiefelhagen, G. Heessels-Gürboğa, J. E. S. van der Hoeven, N. A. Elbers, M. Dijkstra, and A. van Blaaderen, Charging of poly(methyl methacrylate) (PMMA) colloids in cyclohexyl bromide: Locking, size dependence, and particle mixtures, Langmuir **31**, 65 (2015).

[23] M. T. Elsesser, A. D. Hollingsworth, K. V. Edmond, and D. J. Pine, Large core shell poly(methyl methacrylate) colloidal clusters: Synthesis, characterization, and tracking, Langmuir **27**, 917 (2011).

[24] http://www.physics.emory.edu/faculty/weeks//idl/.

[25] Y. Han, N. Y. Ha, A. M. Alsayed, and A. G. Yodh, Melting of two-dimensional tunable-diameter colloidal crystals, Phys. Rev. E **77**, 041406 (2008).

[26] S. C. Kapfer and W. Krauth, Two-Dimensional Melting: From Liquid-Hexatic Coexistence to Continuous Transitions, Phys. Rev. Lett. **114**, 035702 (2015).

[27] D. Goulding and J.-P. Hansen, Effective interaction between charged colloidal particles near a surface, Mol. Phys. **95**, 649 (1998).

[28] R. Aveyard, B. Binks, J. Clint, P. Fletcher, T. Horozov, B. Neumann, V. Paunov, J. Annesley, S. Botchway, D. Nees, A. Parker, A. Ward, and A. Burgess, Measurement of Long-Range Repulsive Forces Between Charged Particles at an Oil-Water Interface, Phys. Rev. Lett. **88**, 246102 (2002).

[29] M. Oettel, Entrapment of charged, nonwetting colloids near oil-water interfaces, Phys. Rev. E **76**, 041403 (2007).

[30] L. Parolini, A. D. Law, A. Maestro, D. M. A. Buzza, and P. Cicuta, Interaction between colloidal particles on an oil-water interface in dilute and dense phases, J. Phys.: Condens. Matter **27**, 194119 (2015).

[31] R. E. Kusner, J. A. Mann, J. Kerins, and A. J. Dahm, Two-Stage Melting of a Two-Dimensional Collodial Lattice with Dipole Interactions, Phys. Rev. Lett. **73**, 3113 (1994).

[32] D. R. Nelson, *Defects and Geometry in Condensed Matter Physics* (Cambridge University Press, Cambridge, 2002), p. 112.

[33] U. Gasser, C. Eisenmann, G. Maret, and P. Keim, Melting of crystals in two dimensions, Chem. Phys. Chem. **11**, 963 (2010).

[34] J. P. Hirth and J. Lothe, *Theory of Dislocations*, 2nd ed. (Wiley, New York, 1982).

[35] P. Dillmann, G. Maret, and P. Keim, Comparison of 2D melting criteria in a colloidal system, J. Phys.: Condens. Matter **24**, 464118 (2012).

[36] J. A. Weiss, A. E. Larsen, and D. G. Grier, Interactions, dynamics, and elasticity in charge-stabilized colloidal crystals, J. Chem. Phys. **109**, 8659 (1998).